sciendo

Civil and Environmental Engineering
Vol. 20, Issue 2, 654-683, DOI: 10.2478/cee-2024-0050

USING FLOW 3D SIMULATION, MULTIPLE NONLINEAR REGRESSION APPROACH, AND ARTIFICIAL NEURAL NETWORK APPROACH APPROACHES TO STUDY THE BEHAVIOR OF VERTICAL DROP STRUCTURES

Hasan AL SHAIKHLI[1,2], Sarah HASHIM MOHAMMED[2,3], Zainab AL-KHAFAJI[4,5*]

[1] Civil Engineering Department, College of Engineering, University of Warith Al-Anbiyaa, Karbala, Iraq. E-mail: e.hassanibraham@gmail.com.
[2] Ministry of Environment, Environmental Protection and Improvement Directorate, Karbala, Iraq.
[3] Air Conditioning Engineering Department, Faculty of Engineering, Warith Al-Anbiyaa University, Iraq.
[4] New Era and Development in Civil Engineering Research Group, Scientific Research Center, Al-Ayen University, Thi-Qar, 64001, Iraq.
[5] Department of Civil Engineering, Universiti Kebangsaan Malaysia, 43600 Bangi, Selangor, Malaysia.
[*] corresponding author: p123005@siswa.ukm.edu.my;

Abstract

The "Vertical Drop" is a hydraulic structure widely utilized in irrigation and wastewater collection systems to equalize height differences between channel slopes and the natural terrain. Previous studies of vertical drops primarily focused on experimental investigations of their hydraulic properties. This study numerically analyzes the hydraulic features of vertical drops with inverse aprons using FLOW3D software and the finite volume method. The volume of fluid (VOF) technique was employed to simulate the free surface. Key flow parameters, such as downstream depth, pool depth, and energy loss, were calculated and validated against experimental data. Various turbulence models and grid configurations were assessed. The numerical results, achieved with a grid size of 20,000 nodes, a downstream channel length of 2 meters, the standard k-ε turbulence model, and a standard wall function, exhibited excellent agreement with theoretical equations. Downstream depth, pool depth, and energy loss closely matched experimental findings. Additionally, numerical impact velocities were compared with empirical equations across different scenarios, demonstrating minimal deviation. These findings confirm that the velocity characteristics of the falling jet can be reliably estimated numerically.

Keywords:

Vertical Drop;
Numerical models;
CFD;
FLOW 3D;
MNLR;
ANN.

1 Introduction

A vertical drop carries water from a higher to a lower height, wasting energy in a pool at the foot. Due to energy loss throughout the descent, the riverbed's slope stays relatively high, conserving its contour. The vertical drop might cause serious structural collapse downstream depending on the structure's proportions and construction. Experts have studied the link between drop size and energy dissipation to construct it more securely. Due to their ease of construction, vertical drops are often utilised to lessen the steep incline and the number of earthworks in drainage and irrigation channels. These structures may have subcritical or supercritical upstream flows. The hydraulic characteristics of vertical drops with subcritical upstream flow have been examined in a number of research. All hydraulic characteristics of the vertical drop were described as a function of the dimensionless number of the drop, which was defined by Rand [1]. Gill [2] examined a drop jet's angle of repose and offered a formula for calculating it.

Rajaratnam and Chamani [3] presented a relationship to estimate energy dissipation and pool depth of vertical drop utilising laboratory data from earlier researchers and their tests. Esen et al. [4] demonstrated that adding a square step to the vertical drop wall equal to the channel's width boosts energy dissipation in comparison to the model without a step. In this regard, models with a 0.6 relative step height to the vertical drop result in an increase of 90percent in energy dissipation. According to Hong et al. [5], increasing the gradient of the bed downstream lengthens the drop's fall.

Utilizing FLUENT software, Farouk & Elgamal [6] looked at the vertical drop. They demonstrated how the pool depth rose as the discharge rose. According to Mansouri and Ziaei (2014), using FLUENT software, a vertical drop with an end threshold dissipated more energy than a straightforward vertical drop. According to Liu et al. [7] analysis of the influence of the upstream gradient of the vertical drop, the pool depth falls as the slope of the upstream bed increases.

Energy dissipation installations have been studied. Al-Shaikhli and Khassaf [8,9] explored the use of CFD for assessing a design, screening, and optimizing hydraulic structures and cofferdam layouts. They also underlined that physical modelling is needed to address poorly understood parts of fluid mechanics. Their article found that CFD optimizes the final conceptual configuration for the project's hydraulics design but advised physical modelling as a final validation.

Gessler [10], described how FLOW 3D models discharge through a vertical overflow drop with freshly calculated maximum flood levels. The discharge findings and falling jet paths were within 5% of prior physical model research. The publication underlined the need for additional validation of CFD models and that this study's results should only be deemed validation for some vertical drop difficulties.

Rajab and Elgizawy [11], developed a study on Manitoba Hydro and Acres Manitoba Ltd. using FLOW 3D to simulate hydropower plant components. The publication described how FLOW 3D matches physical model test findings for discharge, flow patterns, and velocities in modelling a Conawapa diversion port. According to the paper, FLOW 3D can offer discharge measures near empirical estimates for both the Keeyask final vertical drop and diversion ports. The Keeyask project used CFD software to simulate spur groins to minimize cofferdam and surface velocity. Another FLOW 3D experiment is evaluating velocity distributions for two Wuskwatim intake configurations. Modelling the Wuskwatim vertical drop confirmed the structure's hydraulic performance. The analysis concluded FLOW 3D's capacity to simulate early design difficulties.

Ho et al. [12], reviewed FLOW 3D's use in eight Australian vertical drop improvement projects. Their analysis found that numerical model flow rates at head levels equal to or higher than the design level overestimate physical models by 5%. Although certain pressure changes may come from grid resolution constraints, CFD pressures generally accord with physical model data. They determined that CFD is a feasible tool for designing and repairing vertical drops. Further benchmark testing against existing data or design guidelines (USACE - WES) boosted trust in the analytical approach when applied to varied settings or difficulties.

Researchers and hydraulic engineers are always seeking for methods to maximise energy dissipation downstream of these structures and reduce the cost of building a stilling basin, according to investigates of supercritical flow-producing structures like vertical drops. Consider the horizontal serration at its edge may induce turbulence by flowing flow between and between the serrations because the effective component in vertical drop energy dissipation is turbulence formed within the pool. In the current work, the influence of the horizontal serrated edges on the energy dissipation of the vertical drop is examined numerically utilizing FLOW-3D software. Artificial intelligence techniques are increasingly being used to forecast hydraulic structural characteristics. Studies have shown that these techniques provide reliable hydraulic parameter estimates. This research indicated that CFD modelling has to be applied to more vertical drop geometries and combinations. Correlations between physical and numerical model findings would boost software trust and make it a viable alternative to physical modelling in certain situations. In certain cases, the most optimum design strategy may be combining a mix of CFD and physical modelling [13].

This study's main aim is to formulate a new mathematical equation that describes flow behaviour over vertical drop structures. To reach this aim pi theorem applied to form dimensionless groups that govern such hydraulic behaviour. The mathematical equation produced by SPSS 22 software as a multiple nonlinear regression model with a reasonable confidence level, then the Statistical model verified by Artificial intelligence (artificial neural network) regression coefficient of ANN is less than MNLR model, so, ANN used to verify the SPSS model, that depends on the transfer of the input data to the hidden layer and the output layer by a sigmoid function. Finally, a statistical analysis was made to investigate the ability to produce equations to predict the hydraulic behaviour of vertical drop structures.

2 Determine the Suitable Mesh Size

Mesh and cell size are critical parts of any numerical model simulation, so that the size can affect accuracy and time. It was crucial to reduce the cells to occupy critical geometry features and adequate flow details by starting with a comparatively large mesh and then reducing it until the output no longer changed significantly with further mesh size changes. Flow3D enabled the user to use more than one mesh, which made meshing easier. The suitable mesh can be determined by two methods, the first one by using the equation that satisfy the stability limits to not exceed the time step, the second one by using try and error method which is best and fast way and gives a real result. This procedure began with a consistent (0.08 m) mesh cell size. Restart free overflow simulations using a uniform (0.06m) and (0.04m) grid where discharge is the primary desired model outcome. This method allows the model to capture the geometry and flow information across vertical drop bodies without increasing simulation timeframes [14]. FLOW 3D mesh generator utilizes FAVOR to handle complex geometries in Cartesian or cylindrical meshes. Fig. 1 shows how to simplify FLOW 3D meshing. Orthogonal mesh only [15].

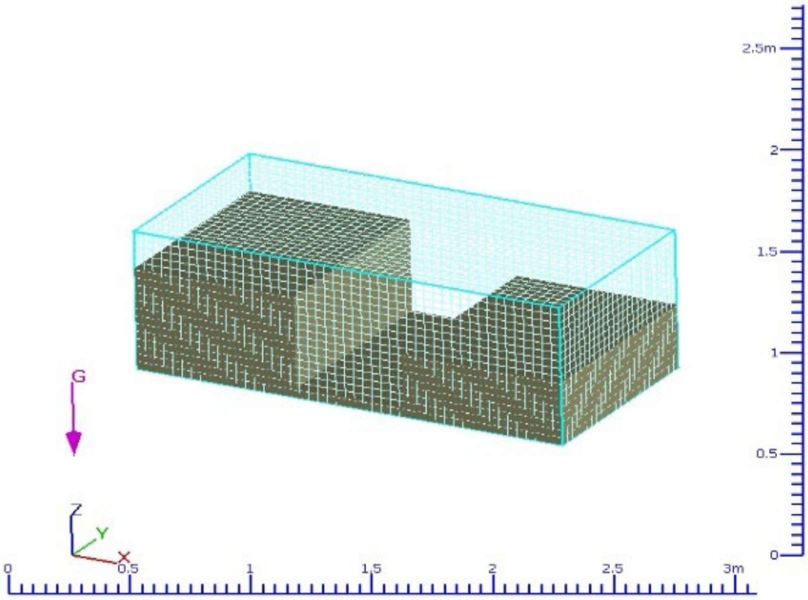

Fig. 1: Mesh generations by FAVOR

3 Numerical Model Set-Up

All vertical Drop simulations used comparable model setups. Each global tab has one fluid, incompressible flow and a free surface or sharp interface. All simulations used water at 20°C for fluid characteristics. Several other model parameters stayed unchanged and will be examined later.

FLOW 3D's previous vertical Drop models have different model geometry. Depending on the experimental investigation, the simulation geometry was delivered as an Auto CAD stereolithographic (STL) picture produced in STL format. STL photos are loaded into FLOW 3D to produce the mesh. Fig.2 shows vertical drop geometry. The usual concrete roughness value for all models' geometry was assumed to be ignored and the component of geometry remained at standard.

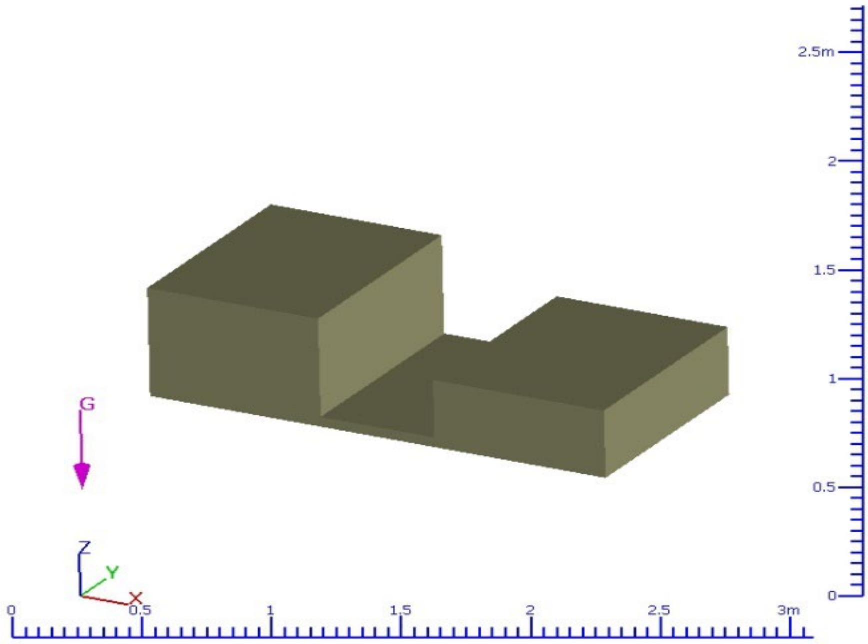

Fig. 2: Vertical drop model imported to FLOW 3D.

In mesh block (1), free surface flow data was sought; thus, the top boundary was set to air pressure and the bottom to symmetry. For the vertical or z-direction mesh extent, the bottom boundary was placed just below the model inlet form to represent the channel bed, and the top boundary was set just above the peak water height. The upstream barrier was established as a specific pressure with fluid height to make the simulation comparable with experimental findings. In these simulations, the downstream border was set to outflow; however, there were other alternatives, such as defined velocity. Upstream x- and y-direction mesh was symmetrical. The initial state was the fluid area in the upstream border and hydrostatic pressure at the top of the mesh block (1). Fig. 3 shows the vertical drop model beginning and boundary conditions. The boundary conditions used in this article was selected as it is no change in its values, also the symmetrical boundary selected as no slip boundary, the time step is different from one run simulation to anther because each one has different flow conditions.

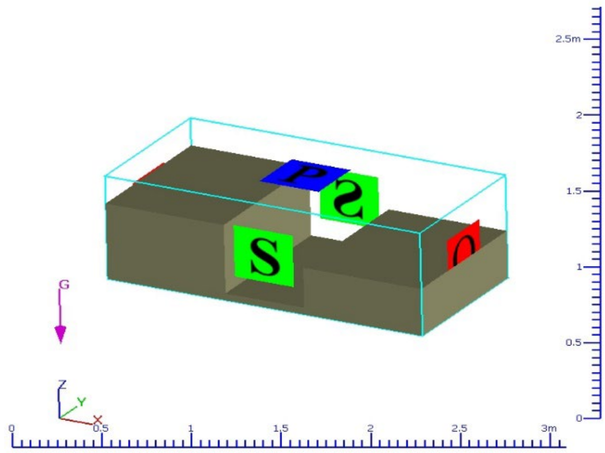

Fig. 3: Boundary and initial conditions for vertical drop model

3.1 Grid sensitivity

The cubic form of grid cells in FLOW 3D software is one of the effective variables in the simulation process and its advancement; thus, the grid cells were picked with varied dimensions to determine which cell size meets the phenomena parameters. Fig. 4 compares flow rating curves for cells ranging from 3 to 8 mm.

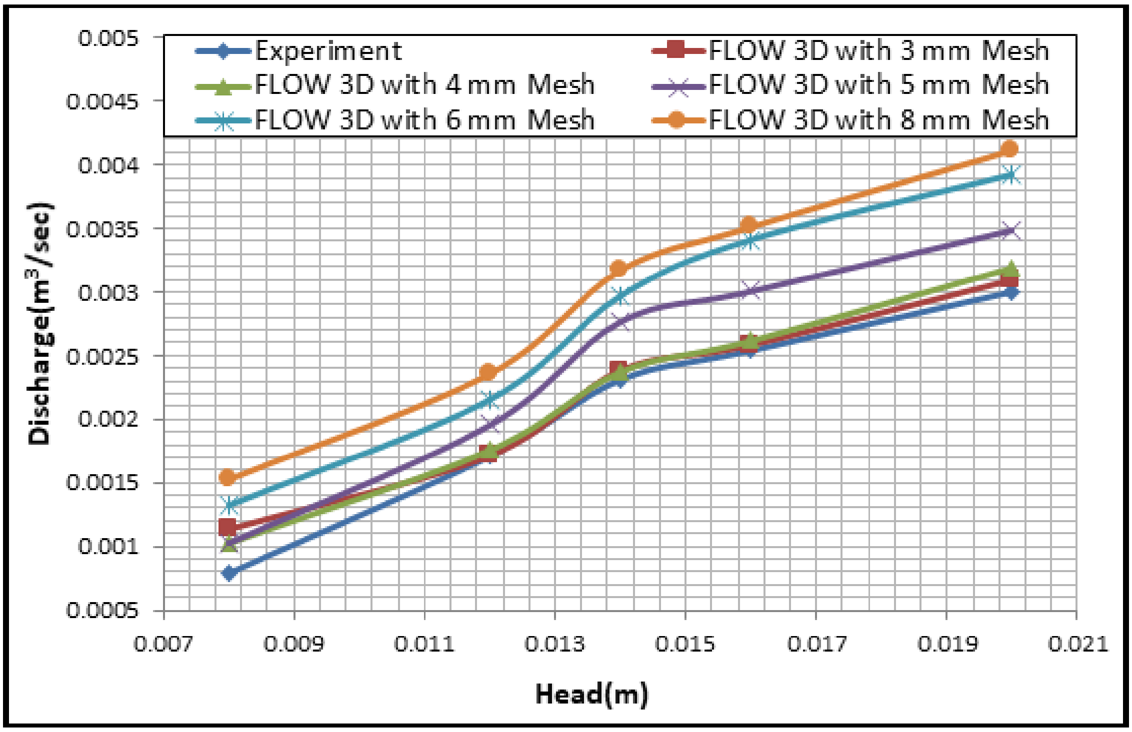

Fig. 4: grid sensitivity test to cell size.

The processes needed to use CFD to analyse a fluid issue are shown in Fig. (5). The physical characteristics of the fluid are first described. The mechanics of the fluid flow are then described using Navier-Stokes equations. By discretizing Navier-Stokes formulas that use the finite volume, finite element, or finite difference methods, they may be solved. The discretization method breaks the issue domain up into several little pieces. Algebraic equations that have been discretized are then solved. The simulation results may then be acquired, examined, and put in a comparison with laboratory studies. The procedure is continued until a satisfying and accurate solution is discovered when the results are insufficient or inaccurate to fix the issue.

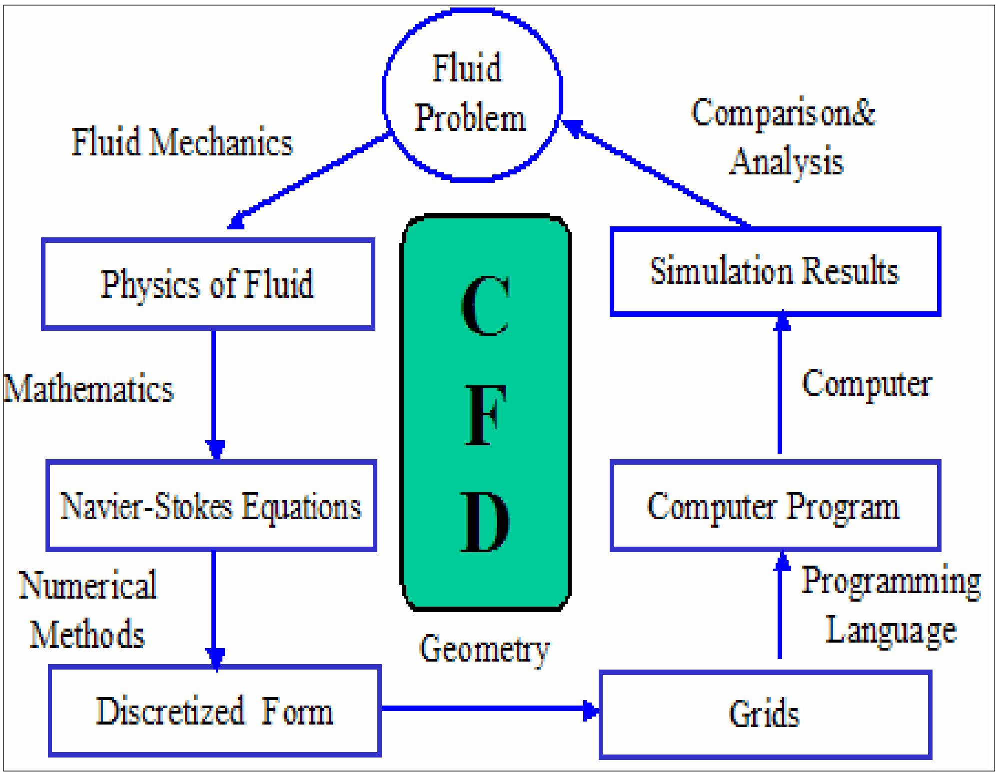

Fig. 5: Process of CFD.

4 FLOW 3D Results

4.1 Energy dissipation

Fig. 6 shows the three-dimensional output of FLOW 3D for the studied models. Each Fig. shows the Energy dissipation over the dimensions of the model.

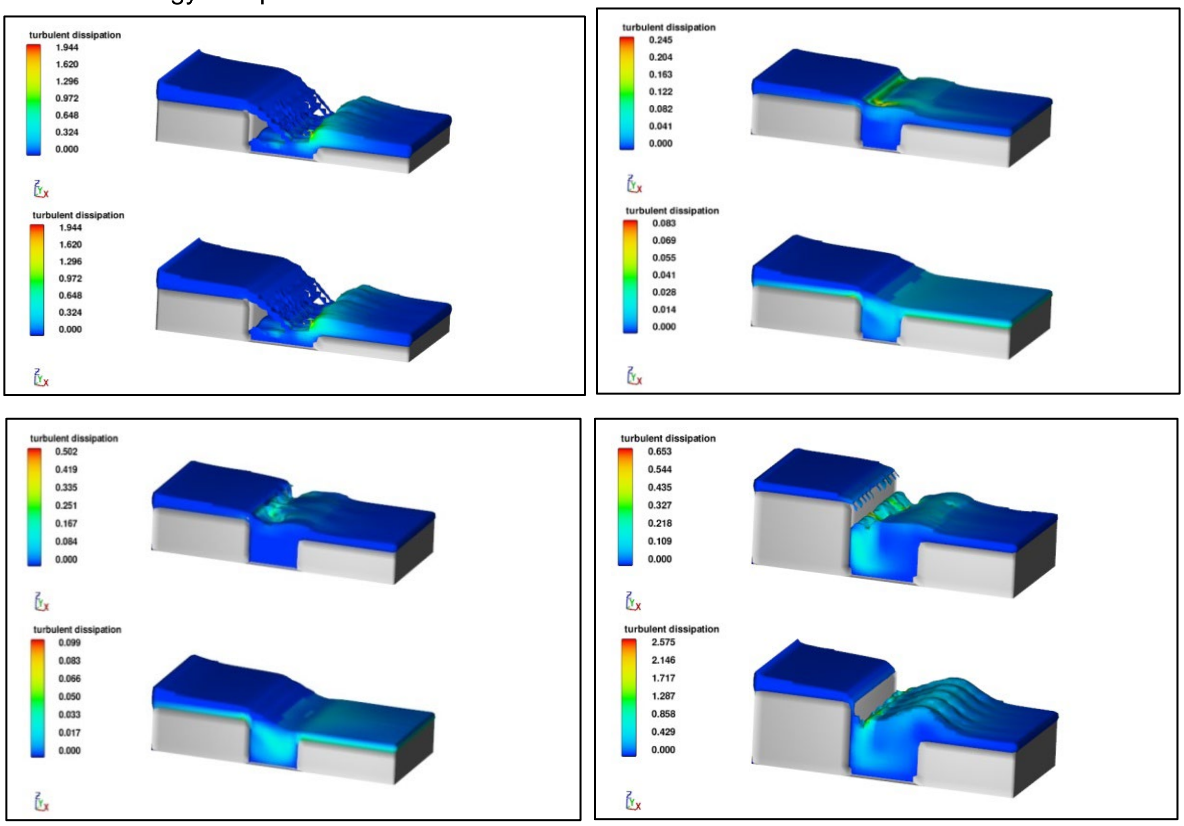

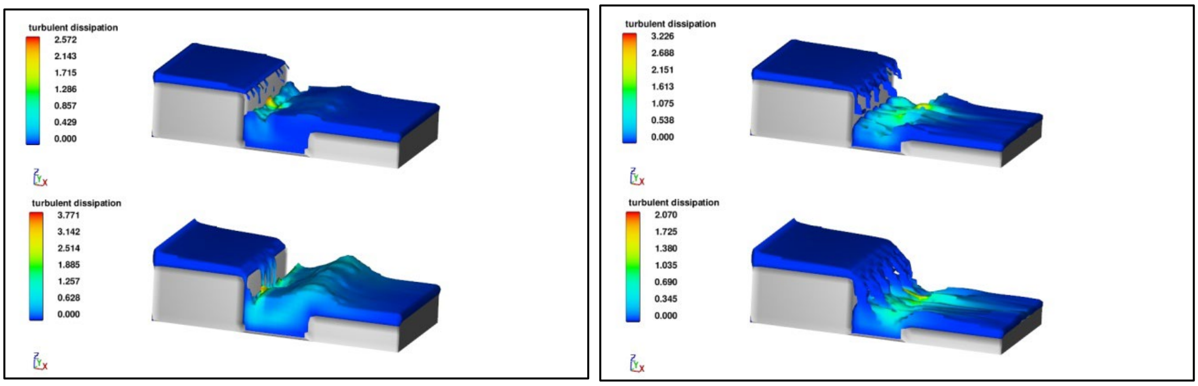

Fig. 6: Flow 3D outputs of Energy dissipation

4.1.1 Flow depth and the average velocity

Figs. 7 and 8 show the three-dimensional output of FLOW 3D for the studied models. Each Fig. shows the flow depth and average depth velocity over the model's dimensions.

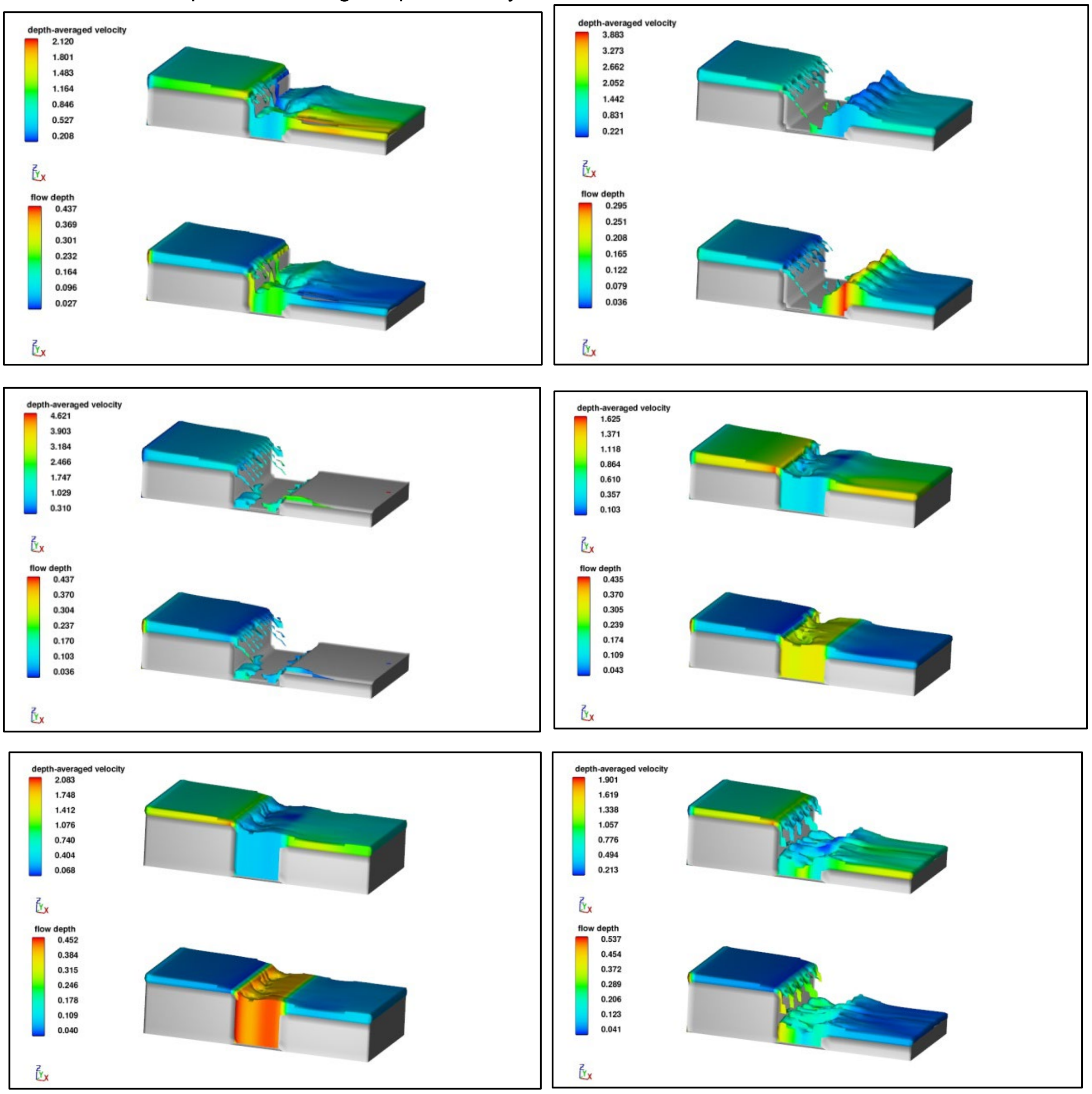

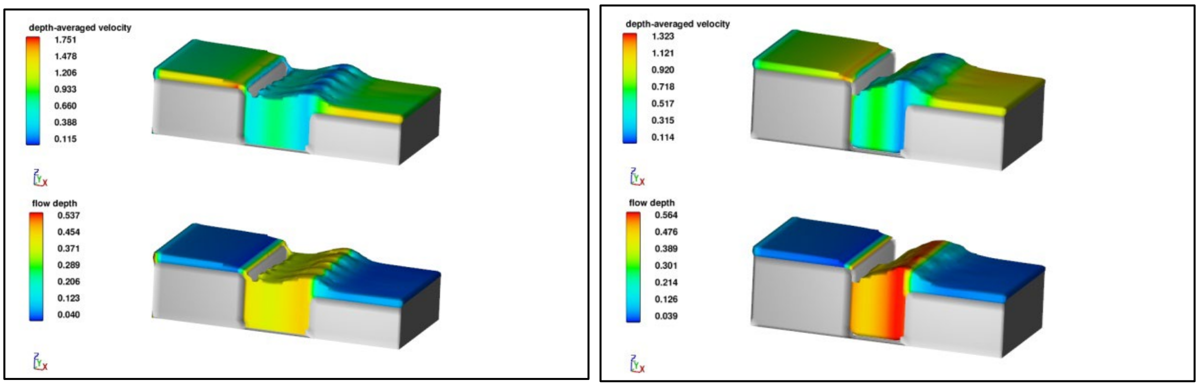

Fig. 7: Flow 3D outputs of flow depth and velocity of H=0.10m

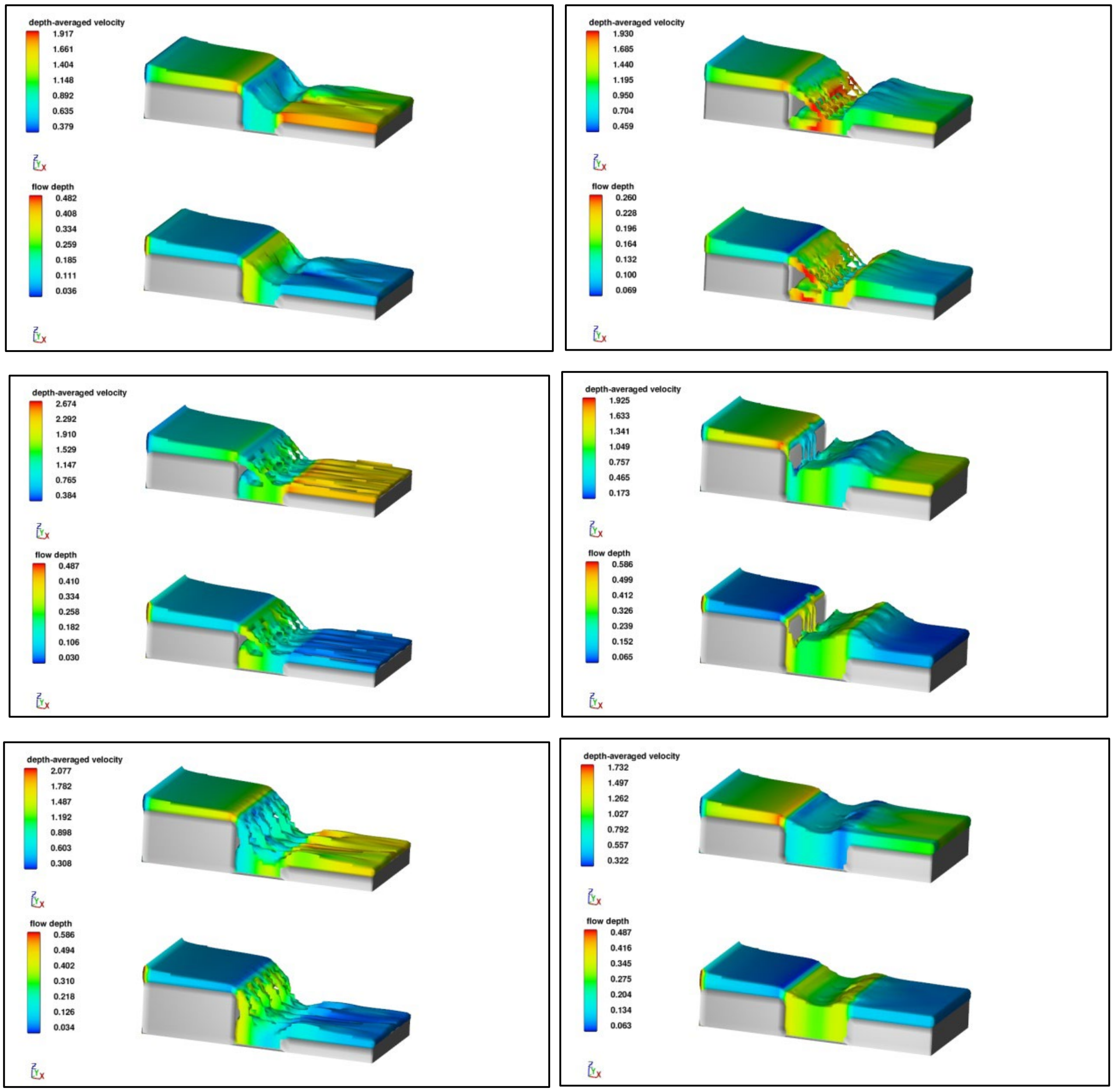

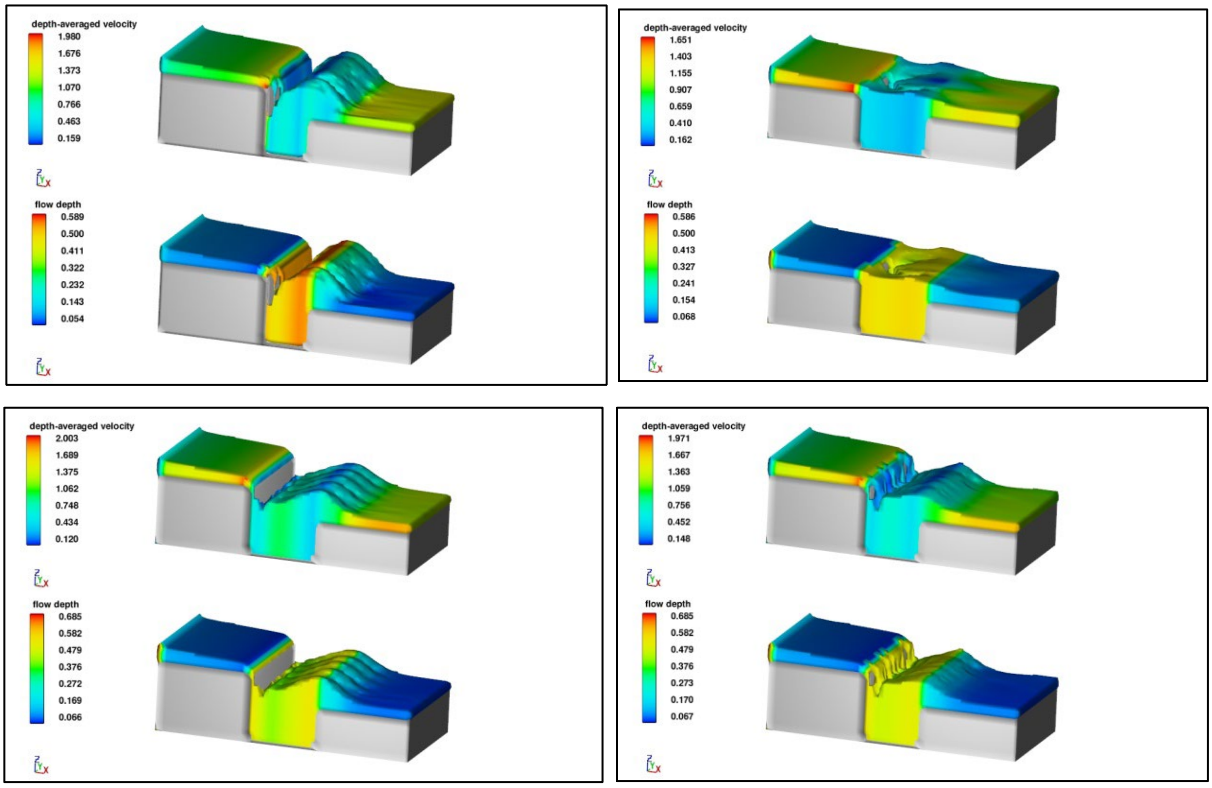

Fig. 8: Flow 3D outputs of flow depth and velocity of H =0.15m

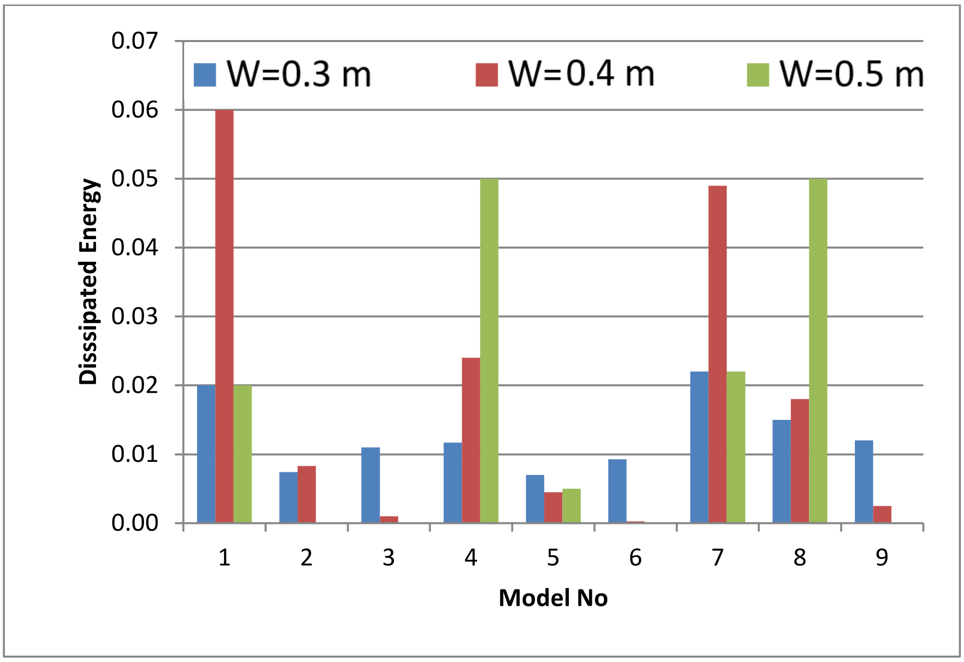

Fig. 9: Flow 3D outputs of 0.05 m head

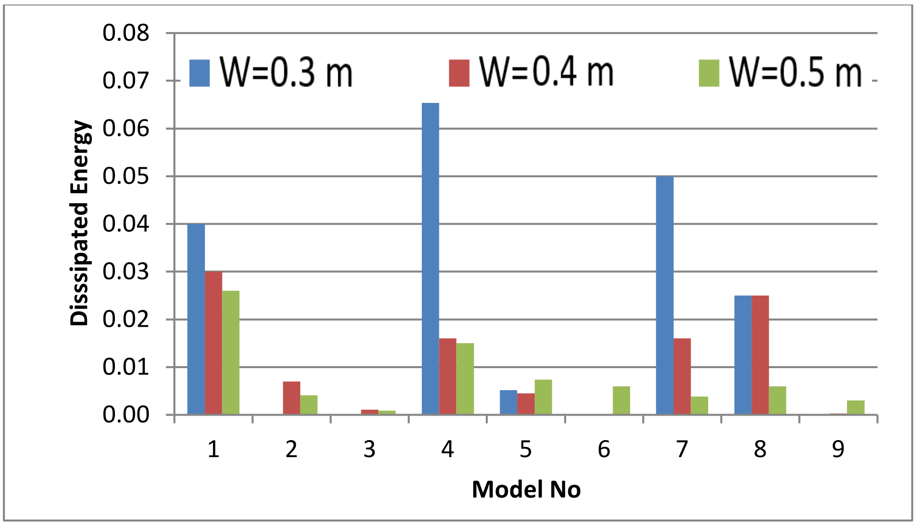

Fig. 10: Flow 3D outputs of 0.1 m head

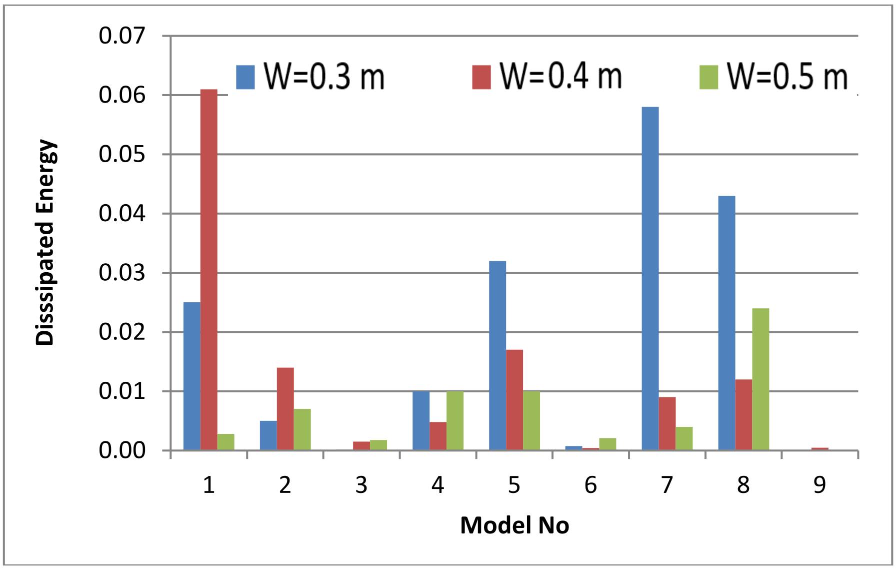

Fig. 11: Flow 3D outputs of 0.15 m head.

Table 1: Outputs of Head 0.05m

No.	Pu Upstream height	Pd Downstream height	W width	y1 Upstream Water level	y2 Downstream Water level	V1 Upstream velocity	V2 Downstream velocity
1	0.30	0.10	0.30	0.05	0.04	0.92	1.83
2	0.30	0.20	0.30	0.05	0.05	0.67	0.92
3	0.30	0.30	0.30	0.05	0.04	0.72	0.88
4	0.40	0.20	0.30	0.05	0.04	0.68	1.07
5	0.40	0.30	0.30	0.05	0.04	1.10	1.20
6	0.40	0.40	0.30	0.05	0.04	0.73	0.92
7	0.50	0.30	0.30	0.05	0.03	0.42	1.00
8	0.50	0.40	0.30	0.05	0.04	0.64	1.16
9	0.50	0.50	0.30	0.05	0.04	0.64	0.83
10	0.30	0.10	0.40	0.05	0.05	0.62	3.23
11	0.30	0.20	0.40	0.05	0.05	0.63	0.84
12	0.30	0.30	0.40	0.05	0.04	0.73	0.90
13	0.40	0.20	0.40	0.05	0.04	0.66	0.95

14	0.40	0.30	0.40	0.05	0.03	0.48	0.88
15	0.40	0.40	0.40	0.05	0.03	0.46	0.63
16	0.50	0.30	0.40	0.05	0.03	0.39	0.51
17	0.50	0.40	0.40	0.05	0.04	0.49	0.60
18	0.50	0.50	0.40	0.05	0.04	0.41	0.59
19	0.30	0.10	0.50	0.05	0.03	0.35	0.47
20	0.30	0.20	0.50	0.05	0.03	0.42	0.65
21	0.30	0.30	0.50	0.05	0.02	0.50	0.72
22	0.40	0.20	0.50	0.05	0.04	0.44	0.76
23	0.40	0.30	0.50	0.05	0.04	0.45	0.47
24	0.40	0.40	0.50	0.05	0.02	0.34	0.52
25	0.50	0.30	0.50	0.05	0.03	0.49	0.61
26	0.50	0.40	0.50	0.05	0.03	0.46	0.95
27	0.50	0.50	0.50	0.05	0.04	0.46	0.17

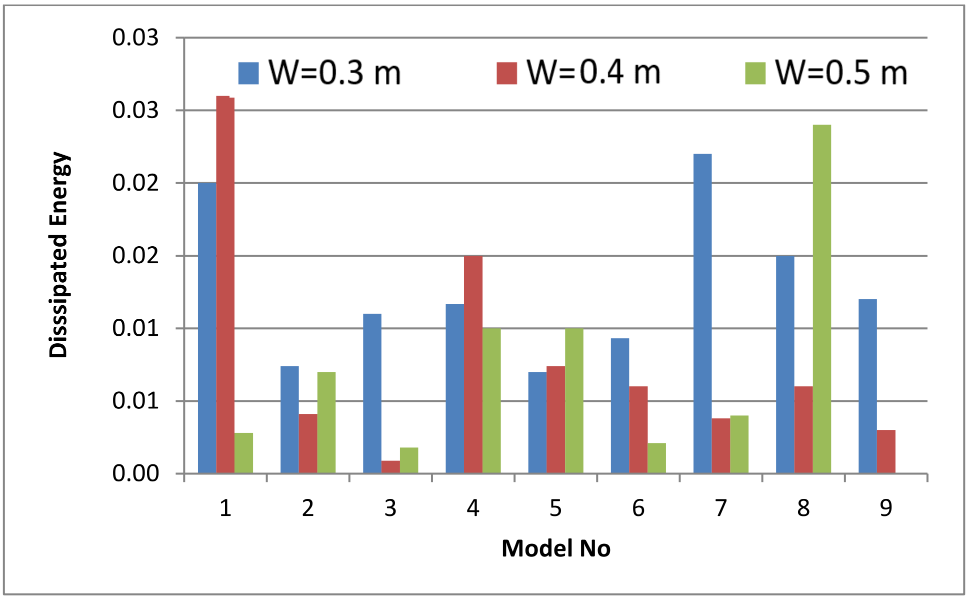

Fig. 12: The effect of width on energy dissipation H=0.05m.

Table 2: Outputs of Head 0.1m

No.	Pu Upstream height	Pd Downstream height	W width	y1 Upstream Water level	y2 Downstream Water level	V1 Upstream velocity	V2 Downstream velocity
1	0.30	0.10	0.30	0.10	0.05	0.50	1.70
2	0.30	0.20	0.30	0.10	0.06	0.50	1.20
3	0.30	0.30	0.30	0.10	0.06	0.70	0.83
4	0.40	0.20	0.30	0.10	0.07	0.72	0.90
5	0.40	0.30	0.30	0.10	0.08	1.14	0.80
6	0.40	0.40	0.30	0.10	0.06	0.86	0.82
7	0.50	0.30	0.30	0.10	0.08	0.66	1.15
8	0.50	0.40	0.30	0.10	0.06	0.73	0.84
9	0.50	0.50	0.30	0.10	0.06	0.59	0.83
10	0.30	0.10	0.40	0.10	0.05	0.50	4.60

11	0.30	0.20	0.40	0.10	0.06	0.60	1.00
12	0.30	0.30	0.40	0.10	0.06	0.70	0.84
13	0.40	0.20	0.40	0.10	0.06	0.72	0.88
14	0.40	0.30	0.40	0.10	0.08	0.66	0.58
15	0.40	0.40	0.40	0.10	0.06	0.64	0.80
16	0.50	0.30	0.40	0.10	0.05	0.66	0.96
17	0.50	0.40	0.40	0.10	0.06	0.72	0.93
18	0.50	0.50	0.40	0.10	0.06	0.55	0.80
19	0.30	0.10	0.50	0.10	0.06	0.56	0.94
20	0.30	0.20	0.50	0.10	0.06	0.72	0.88
21	0.30	0.30	0.50	0.10	0.06	0.68	0.82
22	0.40	0.20	0.50	0.10	0.07	0.66	0.80
23	0.40	0.30	0.50	0.10	0.07	0.65	0.91
24	0.40	0.40	0.50	0.10	0.06	0.58	0.80
25	0.50	0.30	0.50	0.10	0.06	0.65	0.82
26	0.50	0.40	0.50	0.10	0.06	0.66	0.89
27	0.50	0.50	0.50	0.10	0.06	0.59	0.80

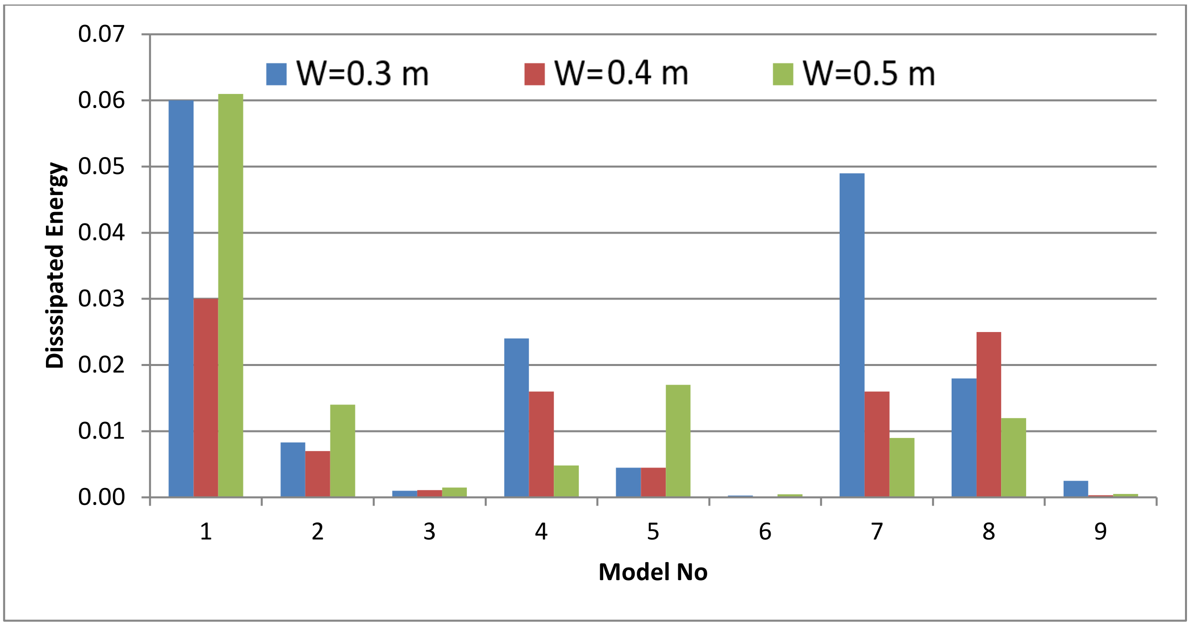

Fig.13: The effect of width on energy dissipation H=0.1m

Table 3: outputs of Head 0.15m

No.	Pu Upstream height	Pd Downstream height	W width	y1 Upstream Water level	y2 Downstream Water level	V1 Upstream velocity	V2 Downstream velocity
1	0.30	0.10	0.30	0.15	0.06	0.60	1.80
2	0.30	0.20	0.30	0.15	0.08	0.63	1.60
3	0.30	0.30	0.30	0.15	0.09	0.80	0.96
4	0.40	0.20	0.30	0.15	0.08	0.90	1.67
5	0.40	0.30	0.30	0.15	0.11	1.20	0.99
6	0.40	0.40	0.30	0.15	0.12	1.00	0.91
7	0.50	0.30	0.30	0.15	0.07	0.80	1.40

8	0.50	0.40	0.30	0.15	0.09	0.93	1.36
9	0.50	0.50	0.30	0.15	0.10	0.82	0.98
10	0.30	0.10	0.40	0.15	0.05	0.60	2.30
11	0.30	0.20	0.40	0.15	0.07	0.62	1.52
12	0.30	0.30	0.40	0.15	0.01	0.81	0.97
13	0.40	0.20	0.40	0.15	0.08	0.83	1.26
14	0.40	0.30	0.40	0.15	0.11	0.90	0.86
15	0.40	0.40	0.40	0.15	0.10	0.86	0.94
16	0.50	0.30	0.40	0.15	0.08	0.89	1.20
17	0.50	0.40	0.40	0.15	0.10	0.89	1.17
18	0.50	0.50	0.40	0.15	0.10	0.81	0.92
19	0.30	0.10	0.50	0.15	0.09	0.66	1.16
20	0.30	0.20	0.50	0.15	0.10	0.93	1.10
21	0.30	0.30	0.50	0.15	0.10	0.79	0.98
22	0.40	0.20	0.50	0.15	0.07	0.83	1.43
23	0.40	0.30	0.50	0.15	0.09	0.91	1.12
24	0.40	0.40	0.50	0.15	0.10	0.79	0.93
25	0.50	0.30	0.50	0.15	0.08	0.80	1.26
26	0.50	0.40	0.50	0.15	0.09	0.83	1.07
27	0.50	0.50	0.50	0.15	0.10	0.75	0.93

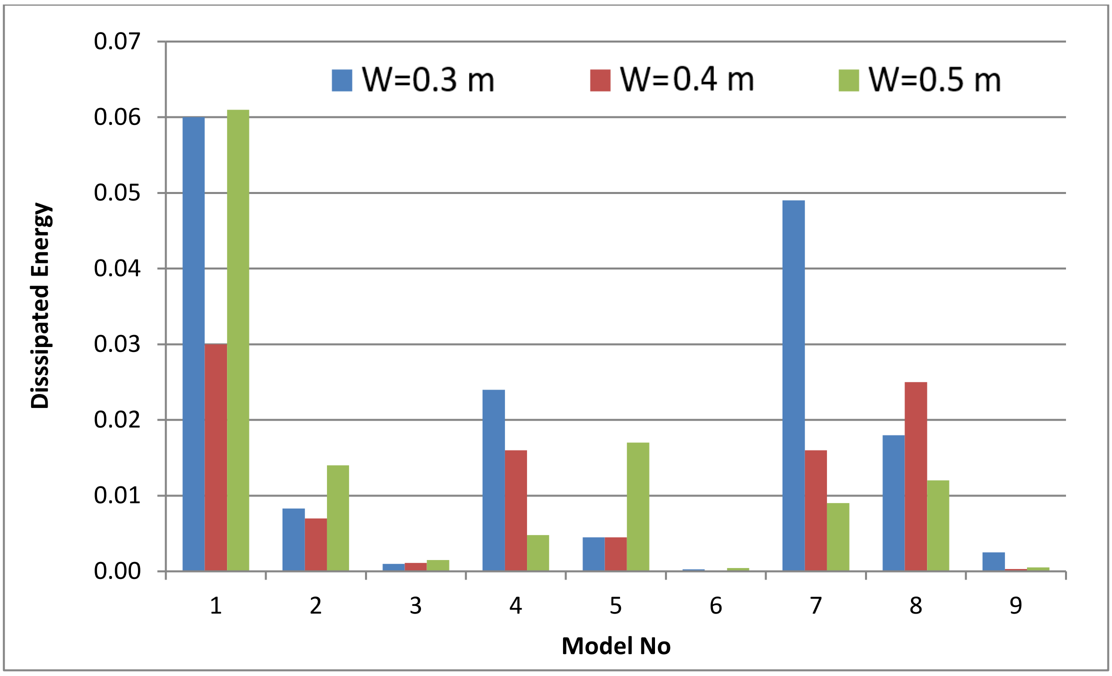

Fig. 14: The effect of width on energy dissipation H=0.15m

4.2 Dimensional Analysis

Dimensional analysis is a powerful method that may be utilized to effectively translate the behaviour of a phenomenon into a mathematical model or an empirical equation. It is only possible to understand the physical regime of the energy dissipation of vertical drop if the correct dimensionless parameters that describe the phenomenon have been set appropriately [16]. The variables that affect the scour in the immediate area can be summed up in equation 1.

$$f(\rho.\mu.V1.y1.V2.y2.E\%.W.P1.P2) = 0 \quad (1)$$

Three repeated factors are selected and fourteen dimensionless sets have been produced using the pi-theorem. The generic equation for the -theorem may be expressed in the form of the Buckingham -theorem, as illustrated in formula 2, where the repeating variables are V1 and y1.

$$f_1(\pi_1.\pi_2.\pi_3.\pi_4.\pi_5.\pi_6.\pi_7) \quad (2)$$

Following the completion of the investigations, the dimensionless groups that emerge as a consequence of Buckingham's theorem are as follows:

$$\pi1 = \frac{P1}{y1}, \pi2 = \frac{P2}{y1}, \pi3 = \frac{W}{y1}, \ \pi4 = \frac{V2}{V1}, \ \pi5 = \frac{y2}{y1}, \ \pi6 = Fr_1, \ \pi7 = E\%$$

In order to simplify the general formula and express it as given in formula 3:

$$E\% = f_1\left(\frac{P1}{y1}.\frac{P2}{y1}.\frac{W}{y1}.\frac{V2}{V1}.\frac{y2}{y1}.Fr_1\right) \quad (3)$$

4.3 Multiple Nonlinear Regression Approach (MNLR)

The statistical method of multiple non-linear regression was utilized to construct prediction models to estimate the scour depth based on the experimental data, Alshaikhli and Kadhim [17]. The probability that the hypothesized correlations exist is determined by the coefficient of regression (R^2). The IBM SPSS Statistics 22 program was utilized in order to do the calculations necessary to determine the suggested relationships' parameters. It is possible to compute the regression coefficient using the following formula [18]:

$$R^2 = 1 - \frac{\sum_{i=1}^{n}(y_o - y_p)^2}{\sum_{i=1}^{n}(y_o - \bar{y})^2} \quad (4)$$

Whereas the coefficient regression is R^2, the detected magnitude is yo, the forecast magnitude is yp, $\bar{y}$ is the average magnitude of yo, and the data's number is n. The following formula form is proposed to forecast the scouring depth, involving the influence of shapes based on the experimental study:

$$E\% = a\left(\frac{P1}{y1}\right)^b\left(\frac{P2}{y1}\right)^c\left(\frac{W}{y1}\right)^d\left(\frac{V2}{V1}\right)^e\left(\frac{y2}{y1}\right)^f(Fr_1)^g \quad (5)$$

The following formula was reached after utilizing the SPSS software to analyse the experimental data:

$$E\% = 0.104 * \left(\frac{P1}{y1}\right)^{0.214} * \left(\frac{P2}{y1}\right)^{-0.041} * \left(\frac{W}{y1}\right)^{-0.27} * \left(\frac{V2}{V1}\right)^{-0.66} * \left(\frac{y2}{y1}\right)^{-0.571} * (Fr_1)^{-1.73} \quad (6)$$

Where the R^2 of this formula is 0.863. The forecast against detected magnitudes of energy dissipation is demonstrated in Fig. 15.

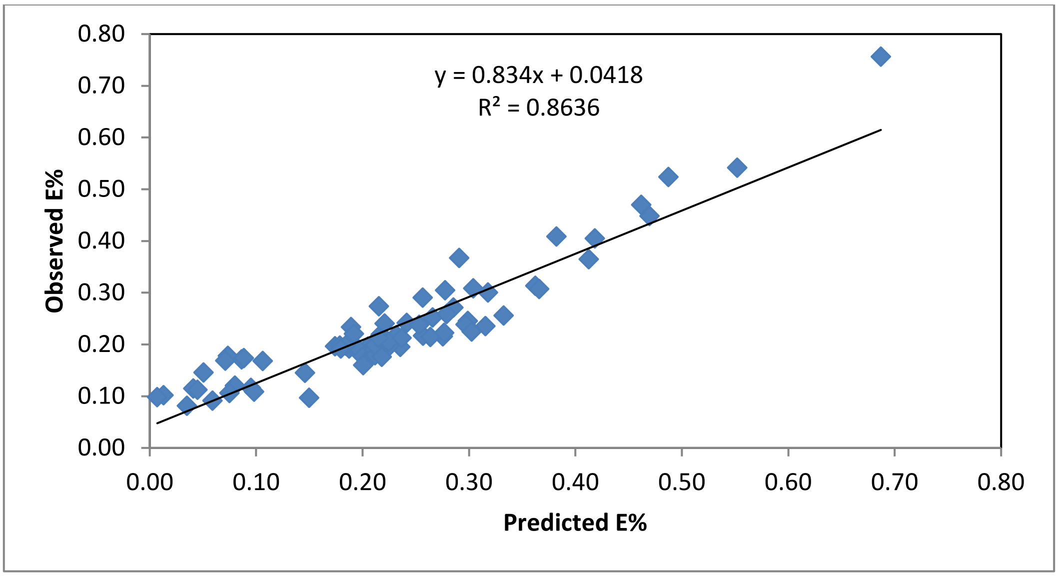

Fig. 15. Predicted- Observed fitted line of MNLR Results.

4.4 Artificial Neural Network approach (ANN)

The nonlinear statistical data modelling techniques are taken into account by the artificial neural network (ANN), a computer system. The most difficult issues may be solved by this technology, which simulates how the human brain analyses and processes information. By extrapolating and interpolating the data, this research use ANN to estimate the scour depth. Alfatlawi and Alshaikhli [9]. Output, hidden, and the input layer inserts the input data into the ANN, while the hidden layer processes the data and determines if there are one or more layers. The complete ANN outcome would then be shown in the output layer. Numerous processing neurons are present in each of these levels.

Each neuron in a layer function similarly in terms of logic. Serial operations are used to convey information from one layer to another. The training technique for neural networks that is most often utilised in literature is the backward and forward rapid propagation algorithm. Researchers utilised the forward kind in this essay. The activation function is a certain mathematical operation that exists in every neuron. This function creates the output for the second layer using the input from earlier levels. The layers are connected by weights. The sigmoid activation function has been employed to describe the data in this study; the Quick Propagation Algorithm (QP) has been utilised to generate weights; and the Multiplayer Normal Feed Forward connection between the neurons of every layer had been utilised to solve and transmit the experimental data (MNFF).

4.4.1 ANN Results

In this work, the local scouring depth experiment data are represented by an activation function that is a sigmoid function. Figs. 16 and 17 demonstrate how the Multiplayer Normal Feed Forward (MNFF) Quick Propagation Algorithm (QP) is employed to compute the weights of the artificial neural network (ANN) and the connection lines between ANN neurons for transferring and solving the data in every layer of the ANN structure (ANN). The input layer consisted of six neurons witch each one represents a dimensionless group that recognized from PI theory to meet the same number of input variables, the first one from the top represent $P1/y1$ and the second one is $P2/y1$ and so on, also the final one is Fr. The hidden layer selected as six neurons because this number of layers is the optimum one to give the output in high precision with small time, the output layer is one neuron only same the output of physical phenomena nominated as E%. The forecasting-observed fitting line of the ANN model with R^2 = 0.9978 is shown in Fig. 18.

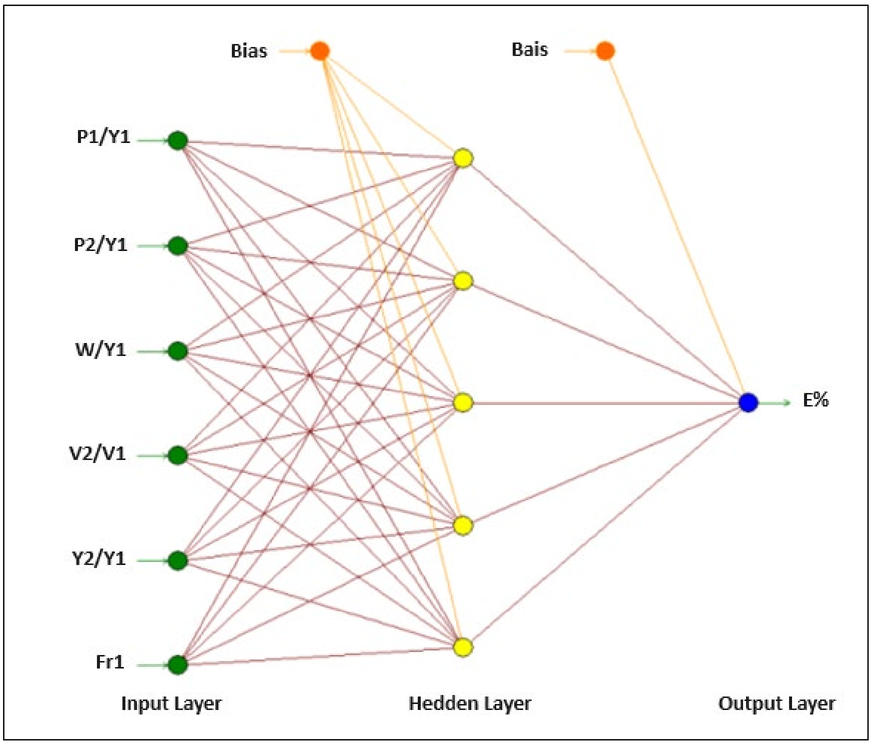

Fig. 16. Local scour structure for artificial neural network.

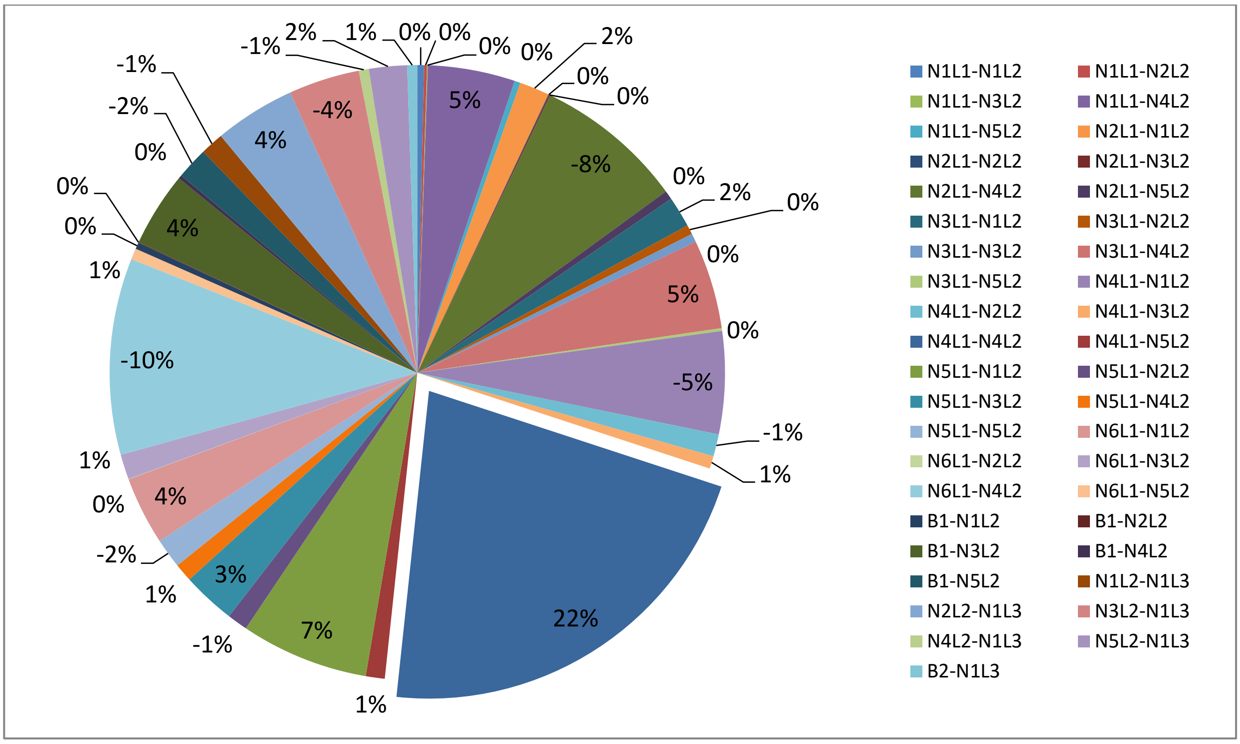

Fig. 17. Pie chart distribution results of neural connection weights.

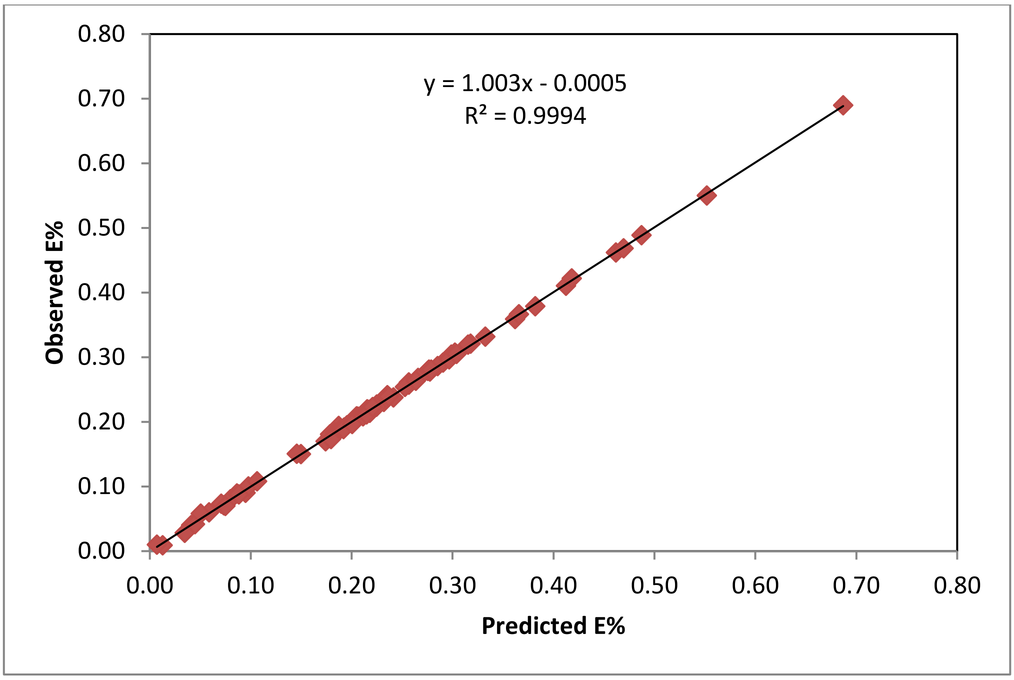

Fig.18. Predicted- Observed fitted line of ANN Results.

4.5 Statistical Analyses

For every model, the statistical analyses must take into account assuring the effectiveness and sufficiency of these outcomes in order to obtain confident findings. The scour depth findings of every model were examined and statistically analysed with the help of some performance indicators and the goodness of fit test in order to understand the behaviour of all independent variables and their associations with the dependent variable; these indicators can be summed up in formulas 8, 9, 10, 11, 12 and 13:

Mean Square Error:

$$MSE = \sum (X - Y)^2 / N \tag{8}$$

Root Mean Square Error:

$$RMSE = \sqrt{MSE} = \sqrt{\sum (X - Y)^2 / N} \tag{9}$$

Relative Square Error:

$$RSE = \sum (X - Y)^2 / \sum (\bar{Y} - Y)^2 \tag{10}$$

Root Relative Square Error:

$$RRSE = \sqrt{RSE} = \sqrt{\sum (X - Y)^2 / \sum (\bar{Y} - Y)^2} \tag{11}$$

Mean Absolute Error:

$$MSE = \sum |(X - Y)| / N \tag{12}$$

Relative Absolute Error:

$$RSE = \sum |(X - Y)| / \sum |(\bar{Y} - Y)| \tag{13}$$

Where X refers to the detected magnitudes, Y refers to the predicted magnitudes, N refers to the magnitudes number, and $\bar{Y}$ refers to the average of predicted magnitudes, where the fit test findings goodness was demonstrated in Table 4.

One of the most frequent tests is the fit test goodness, which may be represented by the summation square error proportion and the R^2 determination coefficient. As illustrated in formula 14, the determination coefficient is a mathematical formula that deals with the proportion of mistakes arising from detected data to errors resulting from projected data.

$$\boldsymbol{R^2 = 1 - (X - Y)^2 / (X - \bar{X})^2} \tag{14}$$

Where X refers to the detected magnitudes, Y refers to the predicted magnitudes, and $\bar{X}$ refers to the average of detected magnitudes.

Table 4: The fit test findings goodness

Parameter	MNLR	ANN
MSE	0.002	0.000
RMSE	0.047	0.003
RSE	0.172	0.001
RRSE	0.414	0.024
MAE	0.038	0.002
RAE	0.497	0.026
R^2	0.862	0.997

5 Conclusions

Depending on the findings of this investigation, the conclusions could be summarized as following:

- It was concluded from this research that the energy dissipation in the vertical drop is completely dependent on the width of the basin when the increase in width of the basin causes an increase in the energy dissipation.
- The difference between the heights of the peaks of vertical drop in the FLOW 3D Software shows that the observed outcomes reached that calculated from the Nieves- Stock equation. So, the increase in head difference causes an increase in energy dissipation.
- According to the CFD results, the increasing head of water over the vertical drop crest causes a decrease in energy dissipation.
- As a result, the FLOW 3D software agrees to simulate the water over vertical drop behaviour with reasonable acceptance.
- The MNLR approach agrees with R2=86%, while 99% is in the ANN approach.
- Pi-theorem can form non-dimensional groups that describe the behaviour of such phenomena.

Acknowledgments

This work was supported by the Civil Engineering Department, Faculty of Engineering, University of Warith AlAnbiyaa, Karbala, Iraq.

Nomenclature

The following symbols are used in this paper:

$\bar{y}$	**Mean Value of y_o**
$\bar{P}$	Modified pressure
y_c	Critical water depth over the crest
C_d	Coefficient of Discharge
CFD	Computational Fluid Dynamics
E%	Energy dissipation rate
E_d	The energy at Downstream of the vertical drop
E_u	The energy at upstream of the vertical drop
FAVOR	Fractional Area/Volume Obstacle Representation
Fr	Froude Number
g	Gravity Force
G	Generation of turbulent kinetic energy
GMRES	Generalized Minimum Residual
H	Head over the inlet crest
h	Height of the step
H_m	Model crest head
H_p	Prototype crest head
k	Turbulence kinetic energy
P	Height from the crest to the bed level of the reservoir
Q	Discharge of the vertical drop
Re	Reynolds Number
STL	Stereo Lithographic
t	Time
u_i	Velocity component
V	Velocity of inlet
V_1	Upstream velocity
V_2	Downstream velocity
VOF	Volume of Fluid
y_1	Upstream water level
y_2	Downstream water level
ε	Turbulent dissipation rate
μ	Dynamic viscosity of the fluid
ρ	The density of the fluid

References

[1]. RAND, W.: Flow Geometry at Straight Drop Spillways. In Proceedings of the Proceedings of the American Society of Civil Engineers; ASCE, 1955; Vol. 81, pp. 1–13.

[2]. Akram Gill, M.: Hydraulics of Rectangular Vertical Drop Structures. Journal of Hydraulic Research 1979, 17, 289–302.

[3]. RAJARATNAM, N. - CHAMANI, M.R.: Energy Loss at Drops. Journal of Hydraulic Research 1995, 33, 373–384.

[4]. ESEN, I.I. - ALHUMOUD, J.M.; HANNAN, K.A.: Energy Loss at a Drop Structure with a Step at the Base. Water international 2004, 29, 523–529.

[5]. HONG, Y.-M. - HUANG, H.-S. - WAN, S.: Drop Characteristics of Free-Falling Nappe for Aerated Straight-Drop Spillway. Journal of hydraulic research 2010, 48, 125–129.

[6]. FAROUK, M. - ELGAMAL, M.: Investigation of the Performance of Single and Multi-Drop Hydraulic Structures. International Journal of Hydrology Science and Technology 2012, 2, 48–74.

[7]. LIU, S.I. - CHEN, J.Y. - HONG, Y.M. - HUANG, H.S. - RAIKAR, R. V.: Impact Characteristics of Free Over-Fall in Pool Zone with Upstream Bed Slope. Journal of Marine Science and Technology 2014, 22, 9.

[8]. AL-SHAIKHLI, H.I. - KHASSAF, S.I.: CFD Simulation of Waves over Mound Breakwater. Journal of Global Scientific Research 2022, 7, 2283–2291.

[9]. KHASSAF, S.I. - ABBAS, H.A. Study of the Local Scour around L-Shape Groynes in Clear Water Conditions. International Journal of Engineering & Technology 2018, 7, 271–276.

[10]. GESSLER, D. CFD Modeling of Spillway Performance. In Impacts of Global Climate Change; 2005; pp. 1–10.

[11]. RAJAB, H. - Elgizawy, A. Design of Spill Tube with Features for Controlling Air Bubble Generated for Aircraft Applicaitons. Mechanical and Aerospace Engineering presentations 2012.

[12]. BERGA, L. - BUIL, J.M. - BOFILL, E. - DE CEA, J.C. - PEREZ, J.A.G.; MAÑUECO, G. - POLIMON, J. - SORIANO, A. - YAGÜE, J. Dams and Reservoirs, Societies and Environment in the 21st Century, Two Volume Set: Proceedings of the International Symposium on Dams in the Societies of the 21st Century, 22nd International Congress on Large Dams (ICOLD), Barcelona, Spain, 18 June 2006; CRC Press, 2006; ISBN 1482262916.

[13]. AL SHAIKHLI, H.I. - KHASSAF, S.I. Using of Flow 3d as CFD Materials Approach in Waves Generation. Materials Today: Proceedings 2022, 49, 2907–2911.

[14]. CHANEL, P.G. An Evaluation of Computational Fluid Dynamics for Spillway Modeling 2009.

[15]. Flow-Science FLOW-3D User Manual, Version 11 2014.

[16]. MIA, M.F. - NAGO, H. Design Method of Time-Dependent Local Scour at Circular Bridge Pier. Journal of Hydraulic Engineering 2003, 129, 420–427.

[17]. AL SHAIKHLI, H.I. - KHASSAF, S.I. Stepped Mound Breakwater Simulation by Using Flow 3D. Eurasian Journal of Engineering and Technology 2022, 6, 60–68.

[18]. STEHLIK-BARRY, K. - BABINEC, A.J. Data Analysis with IBM SPSS Statistics; Packt Publishing Ltd, 2017; ISBN 1787280705.